

Role of Surface Reconstructions in (111) Silicon Fracture

Delia Fernandez-Torre,¹ Tristan Albaret,¹ and Alessandro De Vita²

¹*LPMCN, Université Claude Bernard Lyon 1 and CNRS UMR 5586, 69622 Villeurbanne, France*

²*King's College London, Department of Physics, Strand, London WC2R 2LS, United Kingdom*

(Received 7 June 2010; published 28 October 2010)

The (111) cleavage in crystalline silicon was investigated by hybrid quantum/classical atomistic simulations showing that its remarkable stability is largely due to asymmetric π -bonded reconstructions of the cleavage surfaces created by the advancing crack front. Further simulations show that the same reconstructions can induce an asymmetric dynamical response to added shear stress components. This explains why $[2\bar{1}\bar{1}]$ upward steps are much more common than $[\bar{2}11]$ downward steps on (111) cleavage surfaces, while “zigzag” cleavage with alternated (111) and (11 $\bar{1}$) facets will still occur in crystal samples fractured under [110] uniaxial loading.

DOI: 10.1103/PhysRevLett.105.185502

PACS numbers: 62.20.mt, 02.70.Ns, 68.35.B-, 71.15.Pd

Brittle fracture is intrinsically a multiscale phenomenon. Upon loading, the elastic energy stored in the whole system is released through a process that ultimately consists of the successive rupture of individual chemical bonds. A necessary condition for brittle fracture is given by the Griffith criterion [1] which states that the elastic energy release rate G should exceed the cost of creating new surfaces for the crack advancement to occur. In real systems this picture must be corrected by lattice trapping effects which arise from the discrete nature of the atomic bonding and lead to higher barriers for crack propagation or closing [2]. At room temperature crystalline silicon is a remarkably brittle material where atomic scale features are expected to play a significant role in the fracture properties since these are highly anisotropic and depend on the main cleavage plane, the crack propagation direction and the crack speed [3]. For instance, in (111) cracks traveling along the $[\bar{2}11]$ direction (Si(111) $[\bar{2}11]$ cracks) at velocities lower than $\sim 800 \text{ ms}^{-1}$, crack tip reconstructions are responsible for crack slowing down and a systematic deviation from the initial cleavage plane [4]. However, in fracture experiments on the rotated (110)[001] crack system loaded under pure tensile mode (mode I), the tip is spontaneously deflected by as much as 35.3° back to (111) propagation planes, possibly arranged in zigzag patterns of alternated cleavage facets [3,5]. This illustrates a most striking property of the Si(111) cleavage planes: at high crack velocities they become stable even in the presence of large shear loading components, while in pure mode I flat, mirrorlike cleaved surfaces are readily produced [6] up to G values as high as 16 J/m^2 .

In spite of all the above, early LEED experiments by Henzler [7] and further STM observations by Feenstra and co-workers [8] revealed steps with a specific orientation on the cleaved, (2×1) π -bond-reconstructed surfaces. These climb “upwards” by an atomic bilayer in the [111] direction while moving along the $[\bar{2}11]$ direction, and are usually denoted as $[2\bar{1}\bar{1}]$ steps, i.e., by the outward normal of the step riser. Interestingly, the specific orientation of these

steps cannot be explained on the basis of static total energy calculations, and their formation mechanism is still a matter of discussion [9]. Indeed, the competing $[\bar{2}11]$ “downwards” step orientation involves forming fewer dangling bonds at the step edge and has a lower energy than the observed $[2\bar{1}\bar{1}]$ step [10]. In all cases, the tendency to form steps appears intriguingly at odds with the remarkable dynamical stability of the Si(111) $[\bar{2}11]$ crack system under shear.

To elucidate these questions we carried out molecular dynamics simulations of the propagating Si(111) $[\bar{2}11]$ fracture system using the quantum/classical “Learn on The Fly” hybrid technique (LOTF) [11]. Our simulations focus on the fast, brittle fracture of silicon during which thermally activated processes are not expected to influence the dynamics as long as the temperature is well below the $\sim 800 \text{ K}$ brittle to ductile transition point [12]. After a short transient regime, the dynamics shows that the interplay between the crack shear stress field and surface reconstruction mechanisms naturally leads to the formation of (2×1) π -bonded chain structures on both cleavage surfaces. Noteworthy, the π -bonded chains are parallel to the crack front on one of the surfaces created by the propagating crack, and rotated by 60° on the opposite one [cf. Figs. 2(d)–2(f)]. At high velocities, the occurrence of surface reconstructions helps maintaining the crack on the (111) cleavage plane. Moreover, the different orientation and formation dynamics of the two reconstructions leads to an asymmetric response of the system to an applied shear load. Depending on the shear load sign, flat and stable (111) facets or $[2\bar{1}\bar{1}]$ steps of specific geometry are, selectively, obtained. These results lift the apparent contradiction between different experimental observations, providing a consistent picture of the fast brittle fracture process in the Si(111) $[\bar{2}11]$ crack system.

In our LOTF simulations the forces acting on atoms are obtained from an “on the fly” fitting procedure [11] in which target forces are provided by different reference

force models whose choice depends on each individual atom's position relative to the advancing crack tip. In the quantum region centered on the tip, the reference forces are evaluated within the framework of density functional theory using the SIESTA package [13]. This region typically includes ~ 300 atoms and extends back on the cleavage surfaces up to 16.5 \AA from the crack tip. Further away from the tip, the reference forces are computed using a modified Stillinger-Weber (SW) classical model [14] tuned to exactly match the DFT lattice constant, and the bulk and shear moduli for crystalline silicon at 0 K. Our Si(111) \times $[\bar{2}11]$ crack system model contains 175, 552 atoms, with dimensions $L_x \approx 67.9 \text{ nm}$ and $L_y \approx 65.7 \text{ nm}$ in the $[\bar{2}11]$ and $[111]$ directions, respectively, and $L_z = 7.63 \text{ \AA}$ in the $[0\bar{1}1]$ crack front direction where periodic boundary conditions are imposed. For all simulated times relevant to this work, this system size is amply sufficient to rule out any perturbation of the crack tip motion caused by elastic waves reflected back from the fixed system boundaries. The initial positions already contain a crack seed located at $(\frac{1}{3}L_x, \frac{1}{2}L_y, 0)$ while the loading of the system is imposed in a uniform-strain fashion by fixing the positions of the upper and lower (111) atomic planes of the system. We performed a set of simulations under mode I loading at $G = 7.4 \text{ J/m}^2$, and a second set of calculations in which a mixed mode I-II loading was achieved by imposing a further $\pm 1.2\%$ shear strain ($\frac{\Delta L_x}{L_y} = \pm 0.012$), giving a slightly higher G value of 7.6 J/m^2 . In these conditions, and starting from a simple choice of atomically relaxed (0 K) tip configurations [15], the simulated cracks quickly enter a fast propagation regime, without showing any low speed instabilities [4]. The system heating up due to lattice trapping effects corresponds in all cases to a temperature smaller than 20 K. We note that brittle fracture experiments in Si were shown to be unaffected by temperature for temperatures up to 300 K [3], so that no thermostat was used in the simulations. More details concerning our methodology and calculation setup are given in the supplementary information [15].

For all the studied loading conditions the crack propagation undergoes an initial transient acceleration regime up to a speed of $\approx 2000 \text{ ms}^{-1}$ while proceeding straight along the $[\bar{2}11]$ direction. On the upper cleavage surface [labeled as U in Fig. 2(a)] this produces a $(2 \times 1)\pi$ -bonded reconstruction with threefold coordinated atom chains aligned on the $[0\bar{1}1]$ direction ($[0\bar{1}1]\pi$ -bonded reconstruction) [16,17]. On the lower cleaved surface (labeled L), buckled structures similar to those already described by Haneman [18] are instead obtained. These different reconstructions reflect the broken (111) mirror symmetry of the diamond structure, and can be understood as consequences of the shear stress field at the advancing tip. The shear stress field measured in the crack vicinity is negative (anticlockwise) above the U surface and positive (clockwise) below the L surface [cf. Fig. 1(a)]. Closer inspection shows that the $[0\bar{1}1]\pi$ -bonded reconstruction is stress

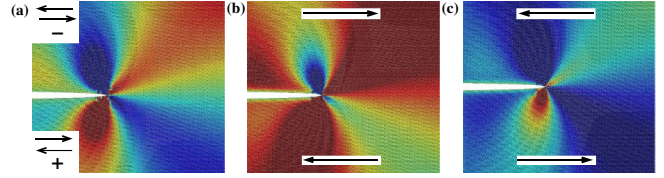


FIG. 1 (color online). Shear stress field plotted in the $(0\bar{1}1)$ plane for the Si(111) $[\bar{2}11]$ cracks at the onset of propagation (see text). The color indicates regions of positive (red), and negative (blue) shear stress. Values out of the range $[-0.005 \text{ MPa}, +0.005 \text{ MPa}]$ are plotted in saturated blue (negative) and red (positive) colors. (a) Mode I loading; the arrows in the insets define positive and negative shear stresses. (b) and (c) Mixed mode I-II loading with positive and negative shear, long arrows indicate the directions of the displacements applied on the boundaries.

compliant on the U surface where it actually occurs in the simulations, and hindered on the L side, where buckled structures form instead in the transient acceleration regime [Fig. 2(c)]. Namely, close to the tip the shear stress field, schematically represented on Fig. 2(a), favors a displacement of the surface atoms in the $[\bar{2}11]$ direction with respect to the subsurface planes on both cleavage surfaces. On the U surface, such a displacement is associated with the $[0\bar{1}1]\pi$ -bonded reconstruction [Fig. 2(b)]. On the L surface the opposite $[2\bar{1}\bar{1}]$ displacement would be needed to promote the $[0\bar{1}1]\pi$ -bonded reconstruction, which is therefore hindered by the shear stress field and, consistently, not obtained in the simulations. Although they are consistent with previous electronic structure calculations [9], the Haneman reconstructions obtained on the L surface do not match experimental observations which report $(2 \times 1)\pi$ -bonded reconstructions on both the cleavage surfaces [17].

This issue is resolved once the system enters a subsequent, more stable propagation regime, after about 2.5 ps from start. Under pure mode I tension, this second regime onsets when the tip velocity exceeds $\approx 2000 \text{ m.s}^{-1}$, and lasts until the simulation ends, while the crack propagates straight along the $[\bar{2}11]$ direction. In this regime a new surface reconstruction mechanism is repeatedly observed on each of the two cleavage surfaces. Snapshots illustrating these reconstructions are shown in Figs. 2(d)–2(f). On the U surface the stress compliant $[0\bar{1}1]\pi$ -bonded surface is generated along the crack path through a bond exchange mechanism only observed at these high velocities ($v_{\text{crack}} \geq 1800 \text{ m.s}^{-1}$), involving the formation of a 7-member ring at the tip [“7RBE” mechanism, Figs. 2(d)–2(f)]. The mechanism proceeds by a $B-C$ bond-breaking step followed by a $B-A$ bond formation. Besides the new 7-member ring, the rebonding leads to the creation of a 6-member ring on the U cleavage surface close to the tip. In a second step, this 6-member ring further recombines with neighboring rings within the quantum region to give the 5/7-member ring structure characteristic of the $[0\bar{1}1]\pi$ -bonded surface.

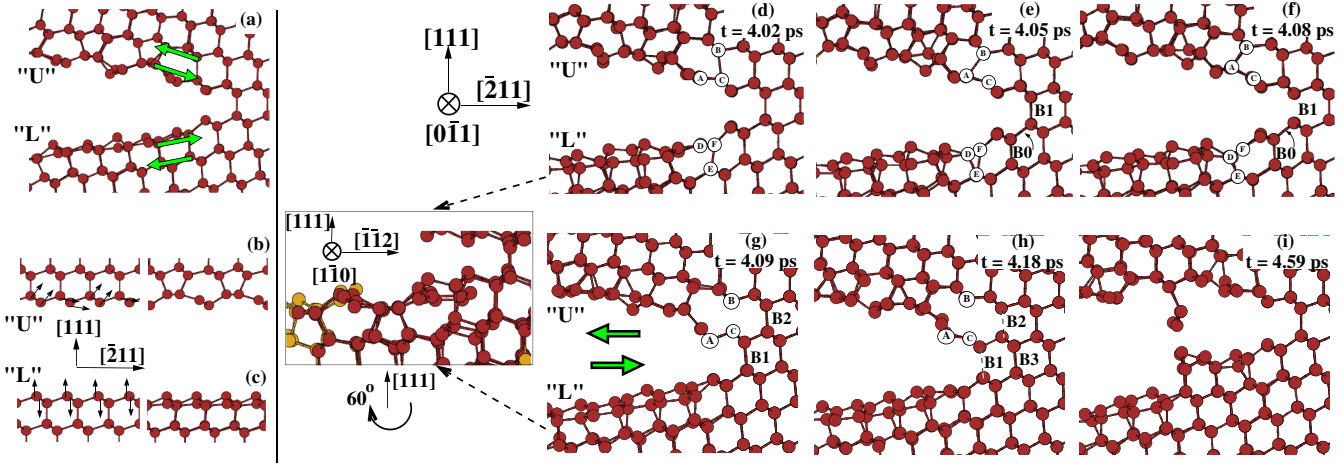


FIG. 2 (color online). (a) Snapshot of the transient regime configuration under mode I: U and L identify inequivalent surfaces, arrows indicate the direction of the shear stress in the surface vicinity; (b) and (c) (111) surface reconstructions in the transient regime on the U and L surfaces respectively: bulk terminated structures are on the left, reconstructed surfaces on the right. The arrows indicate the main atomic displacement direction; (d),(e),(f) Snapshots of the second propagation regime in mode I at $G = 7.4 \text{ J/m}^2$; (g),(h),(i) Snapshots of the $[2\bar{1}\bar{1}]$ step formation in the Si(111) $[\bar{2}11]$ crack system under mixed mode I-II loading ($G = 7.6 \text{ J/m}^2$): the large arrows indicate the displacement corresponding to the applied (negative) shear strain boundary conditions. Inset: view of the L surface reconstructions in the $(1\bar{1}0)$ plane revealing the presence of a π -bonded chain structure along the $[1\bar{1}0]$ direction. The yellow (light grey) atoms in this picture belong to the classical region.

The larger atomic relaxations associated with high speed crack propagation also induce a bond exchange mechanism on the L surface. This starts with the creation of $D-E$ bonds followed by the disruption of $E-F$ bonds. From here on, one $E-F$ bond over two in the $[0\bar{1}1]$ direction is observed to reform during the simulation as the corresponding $D-E$ bond is broken. The resulting structure is easily recognized as a $[1\bar{1}0]\pi$ -bonded reconstruction rotated by 60° around the $[111]$ axis with respect to the one observed on the U surface, as shown in the inset of Fig. 2. The reconstruction involves atomic displacements along the $[\bar{1}\bar{1}2]$ direction, which are stress compliant due to their positive projection over the $[\bar{2}11]$ direction.

To summarize, our first principles computer simulations predict a crack induced “rotated” π -bonded structures on the L surface, consistent with the stress field at the tip and in agreement with the *post-mortem* experimental observations of (2×1) π -bonded chains on both cleaved surfaces [17]. The π -bonded reconstructions on both surfaces involve rebondings with net atomic displacement components along the $[\bar{2}11]$ direction expected to reduce the shear stress in the tip vicinity, effectively stabilizing the formation of (111) cleavage surfaces. This mechanism is observed close to the tip on the L surface where the B_1 bond breaking leading to straight propagation competes with the breaking of B_0 bonds which would lead to step formation. Here, the rebonding of F atoms and their associated $[\bar{2}11]$ displacement components during the reconstruction contribute to lower the stress on the B_0 bond whose disruption is effectively hindered.

We directly tested the stability of this crack system by performing LOTF calculations under mixed mode I-II loading, using a positive shear [Fig. 1(b)] to increase the

likelihood of B_0 -like bond breaking. Using loading conditions corresponding to a shear/tensile strain component ratio as large as 35%, the crack propagates straight along $[\bar{2}11]$ during the entire simulation. The calculated surface structures (not shown) are very similar to those obtained above under pure mode I loading. In particular, rotated π -bonded reconstructions are again observed on the L surface, while no B_0 bond breaking is observed. These results support a physical picture of crack propagation stabilization dynamically promoted by π -bonded surface reconstructions. Consistently, a purely classical simulation carried out in the same loading conditions and using our reference modified SW potential, which produces no surface reconstructions, yielded $[\bar{2}11]$ step formation initiated by B_0 bond breaking. Furthermore, the robust Si(111) $[\bar{2}11]$ crack propagation obtained in our LOTF simulations in spite of a significant positive shear load is consistent with the experimental observation of spontaneous deflection of a Si(110) $[001]$ crack system producing (111) cleavage surface facets [3].

When a negative (anticlockwise) shear load is applied to the system, the local increase of the negative shear stress field further [cf. Fig. 1(c)] promotes the formation of the $[0\bar{1}1]\pi$ -bonded structure on the U surface. In particular, $B-C$ bond breaking is favored and can eventually occur before both the breaking of B_1 bonds and the formation of $A-B$ bonds. As shown in Figs. 2(g)–2(i) the initial $B-C$ bond-breaking induces stress concentration on bond B_2 , which breaks well before B_3 is critically stretched. This completes the formation of a step. We observe several upward $[2\bar{1}\bar{1}]$ steps of this type forming during the simulations. These steps are separated by (111) terraces showing the same $[0\bar{1}1]\pi$ -bonded U surface reconstruction and

rotated $[1\bar{1}0]\pi$ -bonded L surface reconstruction already observed at high propagation speed under purely tensile load. These results are consistent with the $[2\bar{1}\bar{1}]$ steps preferentially observed by STM and LEED experiments in this crack system [7,8].

Our calculations suggest that the formation of these steps is triggered by the time coincidence between the dynamics of the 7RBE reconstruction mechanism on the U surface and the regular $[\bar{2}11]$ crack propagation. This leads to almost simultaneous bond stretching of B - C and B_1 bonds at the tip. Since, in our simulations the 7RBE mechanism only appears at velocities higher than $\sim 1800 \text{ m s}^{-1}$, the $[2\bar{1}\bar{1}]$ steps can be viewed as a high speed crack instability phenomenon. However, the average crack speed is not significantly affected by step formation. This is at variance with what observed in the same system in the case of low speed instabilities, where the occurrence of $[2\bar{1}\bar{1}]$ steps is the result of, and further cause for, crack speed slowing, the positive feedback yielding the formation of macroscopic ridges [4]. Since here the step formation is not coupled to velocity effects, no ridges are predicted, or indeed observed.

While we do not strictly rule out the possibility of forming $[\bar{2}11]$ steps on the L surface, our simulations show that the $[2\bar{1}\bar{1}]$ step is preferred in the Si(111)[$\bar{2}11$] crack system. Although $[2\bar{1}\bar{1}]$ steps were obtained under negative shear in our simulations, we also observed the 7RBE mechanism yielding step formation under pure mode I loading in the high velocity regime. Step formation should therefore be possible in the pure tensile mode, although at a much lower formation rate than if shear strain is applied, while the mechanism could also be promoted by the presence of defects and/or local stress fluctuations in the experimental sample. We finally note that due to its dynamical character, the $[2\bar{1}\bar{1}]$ step formation could not be anticipated by previous static total energy calculations [10]: such an effect is only revealed by a complete description of the dynamics of the π -bonded reconstructions during high speed fracture.

In summary, our simulations show that shear stress present in the crack tip region can drive the formation of π -bonded reconstructions in the silicon (111)[$\bar{2}11$] crack system, consistent with the structures experimentally observed on the cleavage surfaces. The simulations employ periodic boundary conditions along the crack front direction and address the low temperature fracture behavior of perfect crystalline model systems, while no attempt is made to address the more general and complex case of defective samples or temperature regimes close to the brittle to ductile transition. Within these limitations, we consistently find that the broken (111) mirror symmetry leads to different orientations of the π -bonded chains on the cleavage surfaces: parallel to the $[0\bar{1}1]$ crack front on one surface and rotated by 60° on the opposite one. Even if the reconstruction processes on both surfaces act as self-protecting mechanisms that contribute to preserve the $[\bar{2}11]$ direction of propagation, the mentioned asymmetry

is at the origin of a peculiar high speed propagation behavior of the silicon (111)[$\bar{2}11$] system. On the cleavage surface where the π -bonded chains are parallel to the crack front the reconstruction mechanism is sensitive to negative shear components at crack speeds larger than $\sim 1800 \text{ m s}^{-1}$, while it is robust to positive shear loads. This accounts for the selective formation of the $[2\bar{1}\bar{1}]$ steps observed in the experiments. On the contrary, the 60° rotated π -bonded reconstruction is remarkably robust to shear loads of any sign. These results can also explain the observed behavior of the Si(110)[001] fracture system under mode I loading, which exhibits crack deflection on alternated (111) and (11 $\bar{1}$) planes, yielding an intriguing “zigzag” pattern of cleavage surface facets [5]. Here cleavage will occur on both planes under high shear, but in the language of the present work parallel and rotated π -bonded reconstructions will alternately occur on the upper and lower cleavage surfaces of these two planes so that the “stable” positive shear load conditions discussed above are always met. This way largely undefected (111) and (11 $\bar{1}$) facets can be produced and still be consistent with the observed $[2\bar{1}\bar{1}]$ step formation, which preferentially occurs under negative shear.

D.F. and T.A. thank the french ANR grant 05-CIGC: LN3M and IDRIS proj.92293, Lyon1-P2CHPD and CESGA computational centers. A.D.V. acknowledges funding from the EU-FP7-NMP Grant ‘ADGLASS’ and the Rio Tinto Centre for Advanced Mineral Recovery.

-
- [1] A. A. Griffith, *Phil. Trans. R. Soc. A* **221**, 163 (1921).
 - [2] R. Thomson, C. Hsieh, and V. Rana, *J. Appl. Phys.* **42**, 3154 (1971).
 - [3] D. Sherman and I. Be’ery, *J. Mech. Phys. Solids* **52**, 1743 (2004).
 - [4] J.R. Kermode *et al.*, *Nature (London)* **455**, 1224 (2008).
 - [5] R. Pérez and P. Gumbsch, *Phys. Rev. Lett.* **84**, 5347 (2000).
 - [6] J. A. Hauch *et al.*, *Phys. Rev. Lett.* **82**, 3823 (1999).
 - [7] M. Henzler, *Surf. Sci.* **36**, 109 (1973).
 - [8] R.M. Feenstra and J.A. Stroscio, *Phys. Rev. Lett.* **59**, 2173 (1987).
 - [9] T. Hoshi, Y. Iguchi, and T. Fujiwara, *Phys. Rev. B* **72**, 075323 (2005).
 - [10] D.J. Chadi, *Phys. Rev. B* **29**, 785 (1984).
 - [11] G. Csányi *et al.*, *Phys. Rev. Lett.* **93**, 175503 (2004).
 - [12] P.B. Hirsch and S.G. Roberts, *Philos. Mag. A* **64**, 55 (1991).
 - [13] J.M. Soler *et al.*, *J. Phys. Condens. Matter* **14**, 2745 (2002).
 - [14] F.H. Stillinger and T.A. Weber, *Phys. Rev. B* **31**, 5262 (1985).
 - [15] See supplementary material at <http://link.aps.org/supplemental/10.1103/PhysRevLett.105.185502>.
 - [16] K. C. Pandey, *Phys. Rev. Lett.* **47**, 1913 (1981).
 - [17] J. A. Kubby and J. J. Boland, *Surf. Sci. Rep.* **26**, 61 (1996); G. Xu *et al.*, *Phys. Rev. B* **70**, 045307 (2004).
 - [18] D. Haneman, *Rep. Prog. Phys.* **50**, 1045 (1987).